

DENSITY DEPENDENCE OF THE MASS FUNCTION OF GLOBULAR STAR CLUSTERS IN THE SOMBRERO GALAXY AND ITS DYNAMICAL IMPLICATIONS

RUPALI CHANDAR^{1,2}, S. MICHAEL FALL³, AND DEAN E. MCLAUGHLIN⁴

ApJ Letters, in press

ABSTRACT

We have constructed the mass function of globular star clusters in the Sombrero galaxy in bins of different internal half-mass density ρ_h and projected galactocentric distance R . This is based on the published measurements of the magnitudes and effective radii of the clusters by Spitler et al. (2006) in *BVR* images taken with the ACS on *HST*. We find that the peak of the mass function M_p increases with ρ_h by a factor of about 4 but remains nearly constant with R . Our results are almost identical to those presented recently by McLaughlin & Fall (2007) for globular clusters in the Milky Way. The mass functions in both galaxies agree with a simple, approximate model in which the clusters form with a Schechter initial mass function and evolve subsequently by stellar escape driven by internal two-body relaxation. These findings therefore undermine recent claims that the present peak of the mass function of globular clusters must have been built into the initial conditions.

Subject headings: celestial mechanics, stellar dynamics — galaxies: individual (M104, NGC 4594) — galaxies: kinematics and dynamics — galaxies: star clusters

1. INTRODUCTION

One of the most fundamental properties of a system of star clusters is its mass function, defined here such that $\psi(M)dM$ is the number of clusters with masses between M and $M+dM$ [i.e., $\psi(M) \equiv dN/dM$]. There is currently a debate about whether the shape of the mass function of old globular clusters primarily reflects dynamical evolution (Fall & Zhang 2001) or initial conditions (Vesperini et al. 2003). A key observation here is that the turnover or peak of $\psi(M)$ at $M_p \approx (1-2) \times 10^5 M_\odot$ is nearly “universal,” varying little among galaxies of different masses and types and from one location to another within galaxies (Harris 2001). Interpreted naively, these facts tend to favor the scenario in which the present shape of $\psi(M)$ was imprinted when the clusters formed or were relatively young. On the other hand, the observed shape $\psi(M) \approx \text{const}$ below M_p is a clear signature of long-term dynamical evolution driven by internal two-body relaxation (Fall & Zhang 2001; Waters et al. 2006; Jordán et al. 2007).

Another signature of relaxation-driven evolution, recently emphasized by McLaughlin & Fall (2007, hereafter MF07), is that the peak mass should be higher in subsamples of clusters with greater internal densities and thus higher evaporation rates. The expected dependence is roughly $M_p \propto \rho_h^{1/2}$, where $\rho_h = 3M/8\pi r_h^3$ is the mean density within the median (i.e., half-mass) radius r_h . MF07 found essentially this dependence of M_p on ρ_h for the old globular clusters in the Milky Way, and they argued that this, together with the observation $\psi(M) \approx \text{const}$ for $M \lesssim M_p$, provided compelling evidence for the scenario in which dynamical evolution determines the present shape of $\psi(M)$.

In this Letter, we report on a similar study of the old globular clusters in the Sombrero galaxy (M104, NGC 4594). Our goal is to check whether the MF07 findings apply only to the

clusters in the Milky Way or are representative of the clusters in other galaxies. We use the published measurements by Spitler et al. (2006) of the luminosities and effective radii of the globular clusters in images taken with the Advanced Camera for Surveys (ACS) on the *Hubble Space Telescope* (*HST*) as part of the Hubble Heritage Program (GO-9714). The Sombrero galaxy is ideal for this project because it has a large retinue of clusters ($N > 600$), nearly all them are resolved in the ACS images, and there is relatively little contamination by the disk.

2. OBSERVATIONS

The ACS images are arranged in a 3×2 mosaic with overall angular dimensions of $600'' \times 400''$, corresponding to $26 \text{ kpc} \times 17 \text{ kpc}$ at the adopted 9.0 Mpc distance of the Sombrero galaxy. The images are moderately deep; for each pointing, four integrations of 675 s, 500 s, and 350 s were made with the F435W (*B*), F555W (*V*), and F625W (*R*) filters, respectively. Spitler et al. (2006) selected candidate globular clusters based on the following criteria: (i) integrated colors in the ranges $0.9 < B-R < 1.7$ and $0.5 < B-V < 1.1$; (ii) apparent *V* magnitude brighter than 24.3 (roughly the 95% completeness limit); (iii) angular extent at least 0.3 pixels wider than the point-spread function (PSF); (iv) ellipticity less than 0.5; (v) location outside the dust lane; and (vi) visual appearance more like a globular cluster than a star or galaxy. This produced a sample of 659 candidate globular clusters that is believed to be nearly complete brighter than $M_V \approx -5.5$ and nearly free from contamination by foreground stars and background galaxies.

Spitler et al. (2006) present the magnitudes, effective (i.e., half-light) radii r_e , and projected galactocentric distances R of all the clusters in their sample.⁵ We estimate the mass of each cluster from $M = L_V(M/L_V)$, with the total *V*-band luminosity L_V (after correction for Galactic interstellar extinction) and the adopted mass-to-light ratio $M/L_V = 1.5 M_\odot/L_\odot$ (a typical value for old globular clusters in the Milky Way; see McLaughlin 2000). We estimate the internal half-mass

⁵ The quantities denoted here by r_e and R are denoted by R_{hl} and R_{GC} in Table 2 of Spitler et al. (2006).

¹ Carnegie Observatories, 813 Santa Barbara Street, Pasadena, CA 91101

² current address: Department of Physics & Astronomy, University of Toledo, Toledo, OH 43606; Rupali.Chandar@utoledo.edu

³ Space Telescope Science Institute, 3700 San Martin Drive, Baltimore, MD 21218; fall@stsci.edu

⁴ School of Physical and Geographical Sciences, Keele University, Keele ST5 5BG, United Kingdom; dem@astro.keele.ac.uk

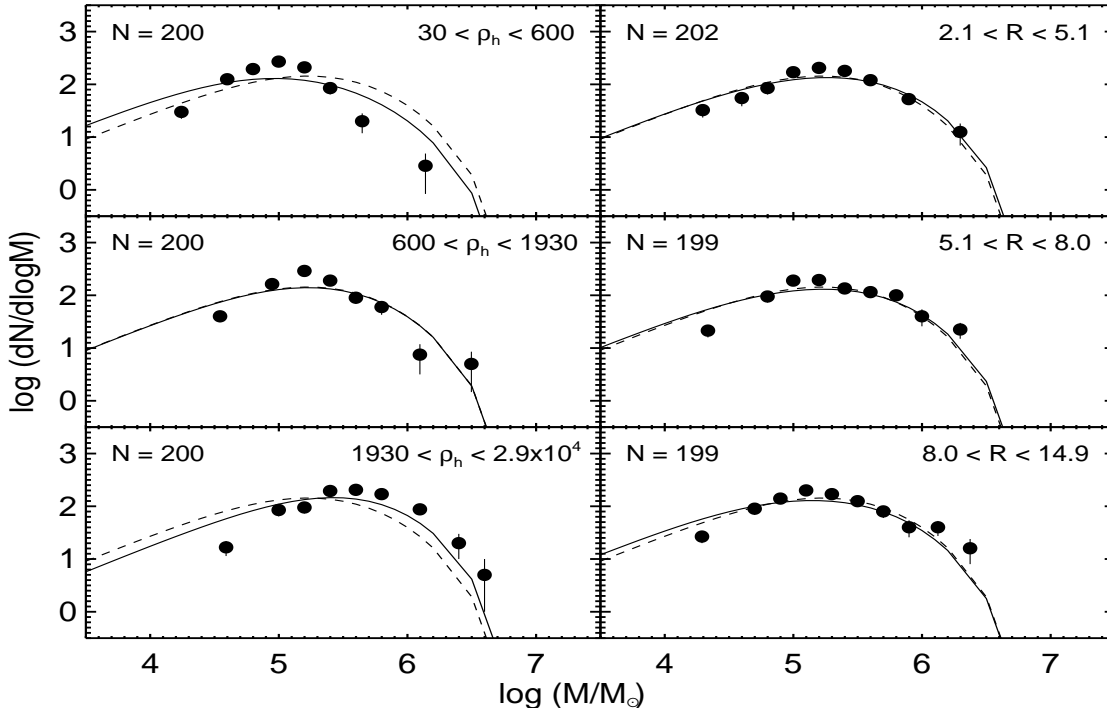


FIG. 1.— Mass function of globular clusters in the Sombrero galaxy. The panels on the left-hand side show three ranges of internal half-mass density ρ_h in units of $M_\odot \text{pc}^{-3}$, as indicated (excluding clusters with $R < 2.1$ kpc). The panels on the right-hand side show three ranges of projected galactocentric distance R in kpc, as indicated (excluding clusters with $\rho_h < 30 M_\odot \text{pc}^{-3}$). The vertical bars represent Poisson (\sqrt{N}) errors. The solid curves were computed from equation (1) as described in the text by summing over terms with individual values of $\rho_{h,i}$ for all clusters in the ρ_h and R bins specified in each panel. The dashed curves, which are the same in all six panels, were computed from equation (1) with a single term with the median value of ρ_h for the full sample of 600 clusters.

density from the definition $\rho_h \equiv 3M/8\pi r_h^3$ and the standard 3D-2D conversion, $r_h = (4/3)r_e$ (neglecting any internal mass/light segregation; see Spitzer 1987).

Figure 1 shows the main results of this paper: the mass function of the globular clusters in the Sombrero galaxy in three bins of internal half-mass density ρ_h (left-hand panels) and three bins of projected galactocentric distance R (right-hand panels). We plot $dN/d\log M$ rather than dN/dM for ease of comparison with the more familiar magnitude distributions. Based on the tests described below, we exclude the 59 clusters with either $\rho_h < 30 M_\odot \text{pc}^{-3}$ or $R < 0.8'$ (2.1 kpc), because the sample becomes less complete at low internal densities (for any R) and small galactocentric distances (for any ρ_h). The mass functions plotted here show the familiar single-peaked shape. What is striking, however, is that the peak mass increases from $M_p \approx 1 \times 10^5 M_\odot$ in the low- ρ_h bin, to $M_p \approx 2 \times 10^5 M_\odot$ in the middle- ρ_h bin, to $M_p \approx 4 \times 10^5 M_\odot$ in the high- ρ_h bin. At the same time, the peak mass remains roughly constant at $M_p \approx 2 \times 10^5 M_\odot$ for all three R bins. Both of these results have high statistical significance and are similar to the MF07 findings for the globular clusters in the Milky Way (see their Fig. 2).

We have replotted Figure 1 with many different binnings in M , ρ_h , and R , and always recover the same result—that M_p increases with ρ_h but is nearly constant with R —to within the statistical uncertainties. We have also made diagrams like Figure 1 for subsamples of clusters divided by color at $B-R = 1.3$ and find only minor differences. This is relevant because the globular clusters in the Sombrero galaxy, like those in many other galaxies, have a bimodal distribution of colors. It is believed that the red, metal-rich clusters ($B-R > 1.3$) are somewhat younger than the blue, metal-poor clusters ($B-R < 1.3$). The spectra of several red and blue clusters indicate, however,

that they are all old, with ages that differ by less than 3 Gyr from each other and from the ages of globular clusters in the Milky Way (Larsen et al. 2002).

We have also made independent measurements of the magnitudes and effective radii of all the clusters in the Spitzer et al. (2006) sample. Our procedure is similar to theirs, with only two minor differences: our measurements of V include r_e -dependent aperture corrections and our measurements of r_e are from the V -band images alone. Both sets of measurements are generally in good agreement, the mean offset (us minus Spitzer et al.) and RMS scatter being only 0.06 and 0.03 in V and 0.04 and 0.07 in $\log r_e$. These small deviations are at the levels expected for the slightly different procedures. As another check, we have inserted artificial clusters with specified properties into the V -band images and measured them in the same way as the real clusters. These experiments indicate that the uncertainties in V and r_e increase, while the completeness of the sample decreases, for diffuse clusters ($\rho_h \lesssim 30 M_\odot \text{pc}^{-3}$) and those near the galactic center ($R < 0.8'$). We have imposed these restrictions on ρ_h and R in most of our analysis (as noted above), but we have confirmed that the relations between M_p , ρ_h , and R are nearly identical in the full Spitzer et al. sample. Finally, we have repeated the entire analysis using only our measurements of V and r_e , and find results that are practically indistinguishable from those based on the Spitzer et al. measurements. These checks give us confidence in our claim that M_p has a significant dependence on ρ_h but not R .

3. MODEL

In this section, we explore the implications of the results displayed in Figure 1. As we have already noted, the peak of the mass function M_p is a factor of about 4 higher in the bot-

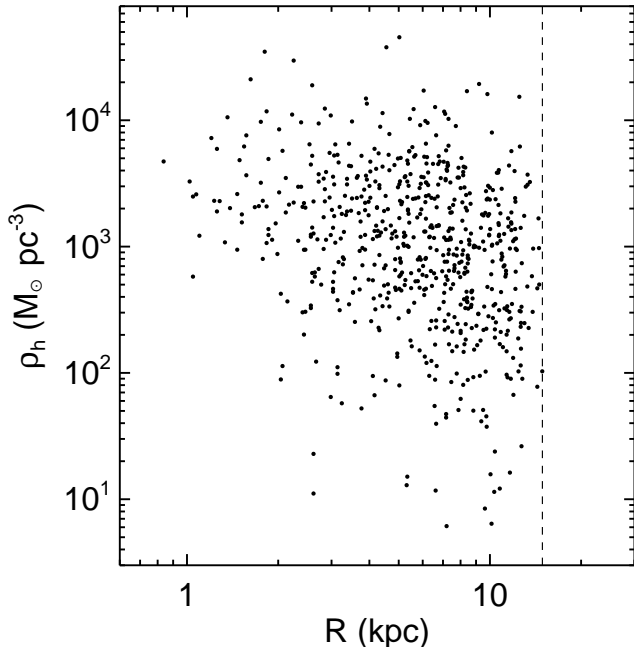


FIG. 2.— Scatter plot of internal half-mass density ρ_h against projected galactocentric distance R for all clusters in the Spitzer (2006) et al. sample. The vertical dashed line shows the maximum value of R accessible in the 3×2 mosaic of ACS images.

tom left-hand panel than in the top left-hand panel, while the median internal density ρ_h within these subsamples increases by a factor of about 13. This is close to the expected scaling $M_p \propto \rho_h^{1/2}$ for relaxation-driven evolution, although the comparison is necessarily crude because the range of ρ_h included in each of the panels is large. The puzzle of why M_p has little or no dependence on projected galactocentric distance R is explained by Figure 2, a plot of ρ_h against R for all clusters in the sample. Evidently, there is a huge scatter and only a mild (anti)correlation between ρ_h and R , thus accounting nicely for the weak dependence of M_p on R despite the relatively strong dependence of M_p on ρ_h . (See Fig. 1 of MF07 for the analogous situation in the Milky Way.)

To make a more precise and informative comparison, we follow the procedure developed by MF07, which in turn is based on the simple (“classical”) model for the escape of stars from tidally limited clusters driven by internal relaxation alone (see Section 3.2 of Spitzer 1987 and references therein). In this model, the mass of each cluster decreases linearly with time, $M(t) = M_0 - \mu_{\text{ev}}t$, where M_0 is the initial mass and $\mu_{\text{ev}} = -dM/dt \propto M/t_{\text{th}} \propto \rho_h^{1/2}$ is the constant rate of mass loss (t_{th} being the half-mass relaxation time). For a population of clusters with the same internal density ρ_h and age τ , the present and initial mass functions are related by $\psi(M) = \psi_0(M + \mu_{\text{ev}}\tau)$ (Fall & Zhang 2001). This implies that the present mass function will have a peak at $M_p \approx \mu_{\text{ev}}\tau$, a low-mass shape $\psi(M) \approx \text{const}$ (for $M \lesssim M_p$), and a high-mass shape $\psi(M) \approx \psi_0(M)$ (for $M \gtrsim M_p$).

For the initial mass function, we adopt the Schechter (1976) distribution, $\psi_0(M) \propto M^\beta \exp(-M/M_c)$, with a power-law exponent $\beta = -2$ and an exponential cutoff at $M_c = 1 \times 10^6 M_\odot$. This choice is motivated by the observed power-law shape of the mass function of young clusters in the Antennae galaxies, $\psi_0(M) \propto M^{-2}$ for $M \lesssim 1 \times 10^6 M_\odot$ (Zhang & Fall 1999), and the fact that the mass functions of old globular clusters

in many galaxies decrease more rapidly than a power law for $M \gtrsim 1 \times 10^6 M_\odot$ (Burkert & Smith 2000; Jordán et al. 2007). We assume this mass function holds at some “initial” time, near the formation epoch but after a brief period of “infant mortality” caused by the activity of massive stars (photoionization, winds, jets, supernovae), since we are concerned here only with the long-term dynamical evolution of the clusters. In our model, this evolution flattens much of the power-law part of $\psi_0(M)$ (for $M \lesssim M_p$) but preserves the exponential part. Thus, fortunately, most of our results are not sensitive to our assumed initial conditions.

The mass function for a population of clusters with a range of internal densities is just the sum of the mass functions for the clusters of each density. From the relations above, we obtain a formula equivalent to equation (3) of MF07:

$$\psi(M) = \sum_i A_i (M + \Delta_i)^{-2} \exp[-(M + \Delta_i)/M_c]. \quad (1)$$

Here, $\Delta_i = (\mu_{\text{ev}}\tau)_i \propto \rho_{h,i}^{1/2}$ is the mass lost over the lifetime of a cluster, $A_i = \Delta_i/E_2(\Delta_i/M_c)$ is the required normalization constant for each term (E_2 being an exponential integral), and the sum is over all clusters in the population. This model is based on the same dynamical evolution and initial conditions as the Fall-Zhang (2001) model, but the internal densities of clusters are no longer coupled to their orbits and hence to assumptions about the space and time dependence of the galactic potential. Thus, equation (1) is equally valid for spherical and triaxial, static and evolving potentials.

We have computed $dN/d\log M = (M/\log e)\psi(M)$ from equation (1) and plotted the results in Figure 1. The coefficient B in the mass-loss formula

$$\Delta_i = B(\rho_{h,i}/10^3 M_\odot \text{ pc}^{-3})^{1/2} 10^5 M_\odot \quad (2)$$

was determined as follows. We first fitted a model with a single term in equation (1)—an “evolved Schechter function” in the nomenclature of Jordán et al. (2007)—to the mass function for the full sample of 600 clusters. The minimum χ^2 occurs for $\Delta = 2.4 \times 10^5 M_\odot$ and hence $\mu_{\text{ev}} = 1.8 \times 10^{-5} M_\odot \text{ yr}^{-1}$ for $\tau = 13$ Gyr. Associating this rate of mass loss with the median internal density of clusters in the full sample, $\rho_h = 1.1 \times 10^3 M_\odot \text{ pc}^{-3}$, gives $B = 2.3$. The resulting “average” mass function for the globular clusters in the Sombrero galaxy is plotted as the dashed curve in each of the six panels of Figure 1. This is very similar to the corresponding function derived by the same procedure by MF07 for the globular clusters in the Milky Way.

We next computed the mass functions for the three ρ_h bins and three R bins from equation (1) with a separate term for each cluster. In doing so, we used the same coefficient $B = 2.3$ derived above for the whole sample to relate the individual values of Δ_i and $\rho_{h,i}$. The results are plotted as the solid curves in Figure 1. These provide good (although not perfect) representations of the observed mass functions, with generally similar shapes and peaks at about the right masses. In particular, the model M_p increases by a factor of about 3 between the low- ρ_h and high- ρ_h bins, while remaining almost constant for the different R bins. The first of these relations is slightly weaker than $M_p \propto \rho_h^{1/2}$ because of the exponential cutoff at $M_c = 1 \times 10^6 M_\odot$.⁶

The observed mass function is slightly narrower or more sharply peaked than the model curves, especially in the left-hand panels of Figure 1. One factor that might contribute to

⁶ The simple scaling $M_p \propto \rho_h^{1/2}$ is exact in the limit $M_c \gg M_p$ (MF07).

this is residual incompleteness for faint (i.e., low-mass) clusters, particularly in the lowest-density bin. Another is our simplifying assumption that all clusters have the same mass-to-light ratio. In reality, there will be a distribution of M/L_V , and this will broaden the mass function somewhat relative to the luminosity function [which we have adopted as a proxy for $\psi(M)$]. A more speculative possibility that would further improve the fits is that the cutoff M_c in the initial mass function might increase slightly with ρ_h instead of remaining fixed as we have assumed here. In any case, it is clear from Figure 1 that our simple, relaxation-driven model captures the essential features of the observed mass function even without these adjustments.

4. DISCUSSION

Our findings for the globular clusters in the Sombrero galaxy corroborate those of MF07 for the globular clusters in the Milky Way. The Sombrero sample is larger ($N = 600$ vs $N = 146$) but, because of the modest sensitivity to extended sources and the restricted angular extent of the *HST* observations, it covers smaller ranges of internal density ($6 \lesssim \rho_h \lesssim 5 \times 10^4 M_\odot \text{ pc}^{-3}$ vs $3 \times 10^{-2} \lesssim \rho_h \lesssim 6 \times 10^4 M_\odot \text{ pc}^{-3}$) and galactocentric distance ($2 \lesssim R \lesssim 15 \text{ kpc}$ vs $0.6 \lesssim R \lesssim 123 \text{ kpc}$). In both galaxies, the peak of the mass function increases with internal density—approximately as $M_p \propto \rho_h^{1/2}$ —but remains nearly constant with galactocentric distance. These relations are consistent with each other because ρ_h correlates only weakly with R . Thus, we now see that whether the peak mass appears “universal” depends crucially on one’s perspective. In terms of galactocentric distance, it may be; but in terms of internal density, the more physically meaningful quantity, it certainly is not.

We have interpreted these observations in the context of a simple, approximate model in which clusters form with a Schechter initial mass function and are subsequently disrupted by stellar escape driven by internal two-body relaxation. Our model predicts present mass functions similar to the observed ones, including the correct dependence on both ρ_h and R . We compute mass-loss rates and hence $\psi(M)$ directly from the observed ρ_h , and only then do we use the observed ρ_h – R distribution to reexpress $\psi(M)$ in terms of R . Our approach completely avoids having to specify the ρ_h – R distribution in the past and thus sidesteps the interesting but difficult problem of explaining physically how the present ρ_h – R distribution came about (which ultimately will require a detailed understanding of the formation and evolution of both galaxies and star clusters). Instead, we assume only that the present ρ_h of extant clusters are good guides to their past ρ_h

and thus to their average mass-loss rates over a Hubble time. For a more complete discussion of these issues, we refer the interested reader to MF07.

Most previous models link the internal densities and hence the mass-loss rates of clusters to their orbits in static, spherical galactic potentials (adopted for analytical simplicity). To account for the observed weak radial gradient in the mass functions of globular clusters, these models are forced to have orbital distributions with strong radial anisotropy at large galactocentric distances, possibly more than is allowed by observations in the Milky Way (Fall & Zhang 2001) and certainly more than allowed in M87 (Vesperini et al. 2003). However, as Fall & Zhang (2001) have emphasized, these conclusions are primarily a consequence of the simplifying assumptions about the galactic potential, not the underlying premise about the disruption of clusters. In more realistic models, galaxies form and evolve by a hierarchical series of collisions, mergers, and other accretion events. Galactic potentials in this case are time-dependent and non-spherical, and the orbital energies and angular momenta of clusters are not conserved. The orbits and positions of clusters are rearranged many times and any initial gradients in M_p or ρ_h are inevitably weakened if not eliminated, consistent with the observations plotted in Figures 1 and 2. By comparison, the idealized models with static, spherical potentials overpredict gradients in M_p and ρ_h and therefore represent a limiting (i.e., “worst-case”) scenario.⁷

Our results also have an important bearing on recent attempts to infer the initial form of the mass function of globular clusters. Vesperini et al. (2003) have advocated a gaussian-like or lognormal initial mass function with a built-in peak near $10^5 M_\odot$ to account for the observed shape and weak radial variation of the present mass function in the context of models with static, spherical galactic potentials (see also Vesperini 2000, 2001). As noted above, this is not the only, or even the most natural solution of this problem. Our model provides a direct counterexample to these claims: an initial mass function with a power-law shape (for $M \lesssim 10^6 M_\odot$) evolves into the present mass function with a peak at $M_p \approx 2 \times 10^5 M_\odot$ and with the observed dependence of M_p on ρ_h and R .

We thank Forrest Hamilton for creating the ACS mosaic images used in this project. Our work is supported in part by NASA grants AR-09539.1-A and GO-10402.05-A. *HST* data are obtained at STScI, which is operated by AURA, Inc., under NASA contract NAS5-26555.

radial transition probabilities or rates.

REFERENCES

- Burkert, A., & Smith, G. H. 2000, *ApJ*, 542, L95
 Fall, S. M., & Zhang, Q. 2001, *ApJ*, 561, 751
 Harris, W. E. 2001, in *Star Clusters* (28th Saas-Fee Advanced Course), ed. L. Labhardt & B. Binggeli (Berlin: Springer), 223
 Jordán, A., et al. 2007, *ApJS*, 171, 101
 Larsen, S. S., Brodie, J. P., Beasley, M. A., & Forbes, D. A. 2002, *AJ*, 124, 828
 McLaughlin, D. E. 2000, *ApJ*, 538, 818
 McLaughlin, D. E., & Fall, S. M. 2007, *ApJ*, submitted (arXiv:0704.0080; MF07)
 Schechter, P. 1976, *ApJ*, 203, 297
 Spitler, L. R., Larsen, S. S., Strader, J., Brodie, J. P., Forbes, D. A., & Beasley, M. A. 2006, *AJ*, 132, 1593
 Spitzer, L. 1987, *Dynamical Evolution of Globular Clusters* (Princeton: Princeton Univ. Press)
 Vesperini, E. 2000, *MNRAS*, 318, 841
 Vesperini, E. 2001, *MNRAS*, 322, 247
 Vesperini, E., Zepf, S. E., Kundu, A., & Ashman, K. M. 2003, *ApJ*, 593, 760
 Waters, C. Z., Zepf, S. E., Lauer, T. R., Baltz, E. A., & Silk, J. 2006, *ApJ*, 650, 885
 Zhang, Q., & Fall, S. M. 1999, *ApJ*, 527, L81